J. Fluid Mech. (1996), vol. 324, pp. 393–406

Free-surface flows with two stagnation points

By J.-M. VANDEN-BROECK[1] AND F. DIAS[2]

[1] Department of Mathematics and Center for the Mathematical Sciences, University of Wisconsin-Madison, WI 53706, USA
[2] Institut Non-Linéaire de Nice, 1361 route des Lucioles, 06560 Valbonne, France

(Received 22 January 1996 and in revised form 13 May 1996)

Symmetric suction flows are computed. The flows are free-surface flows with two stagnation points. The configuration is related to the modelling of wave breaking at the bow of a ship. It is shown that there is a countably infinite number of solutions and that the free-surface profiles are characterized by waves.

1. Introduction

In a recent paper Dias & Vanden-Broeck (1993) presented a model for the spray at the bow of a ship. The bow was assumed to be a semi-infinite flat-bottomed body terminated by a face inclined with the horizontal. The spray was modelled by a layer of water rising along the bow and falling back as a jet (see figures 1*a* and 1*b*).

The solutions were computed by a series truncation procedure. It was found that there is a solution for each value of the Froude number

$$F_d = \frac{U}{(gd)^{1/2}}. \tag{1.1}$$

Here U is the ship velocity, g the acceleration due to gravity and d the draught.

For large values of F_d, the separation point D is on the bow as in figure 1(*a*). As F_d decreases, the separation point D rises along the bow and then moves on the free surface. There are therefore two stagnation points S and D on the free surface (see figure 1*b*). As F_d is further decreased, the distance between the stagnation points D and S increases. However more and more terms in the series representation are needed to compute accurate solutions. Therefore Dias & Vanden-Broeck (1993) presented only solutions for which the distance between the two stagnation points D and S is relatively small.

In this paper we consider another flow for which there are two stagnation points on the free surface (see figure 2). This flow can be created by opening a slit in a flow beneath a flat plate and applying a negative or positive pressure in the slit. There is a vertical wall BC and a horizontal wall AB on the left as in figures 1(*a*) and 1(*b*). There is also a vertical wall ED and a horizontal wall EG on the right. Therefore the configuration of figure 2 can be viewed as an 'approximation' of the flow of figure 1(*b*) in which the dividing streamline DI is replaced by the walls ED and EG. The 'approximation' has the advantage that solutions for which the distance between the two stagnation points is large can be computed. This configuration is also relevant to particular shapes of ships used to launch objects into the sea or retrieve them from the sea. Experiments have shown that the launching or retrieving procedure is easier if it is done through a hole in the middle of the ship rather than from overboard

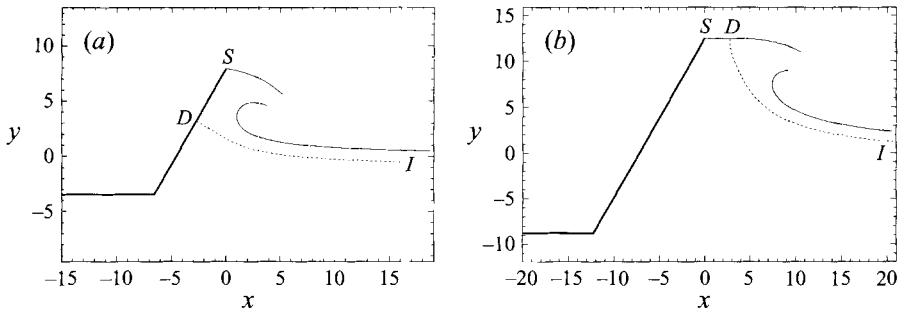

FIGURE 1. Bow flows: (*a*) stagnation point D on the bow, (*b*) stagnation point D on the free surface. The dotted lines represent the dividing streamlines.

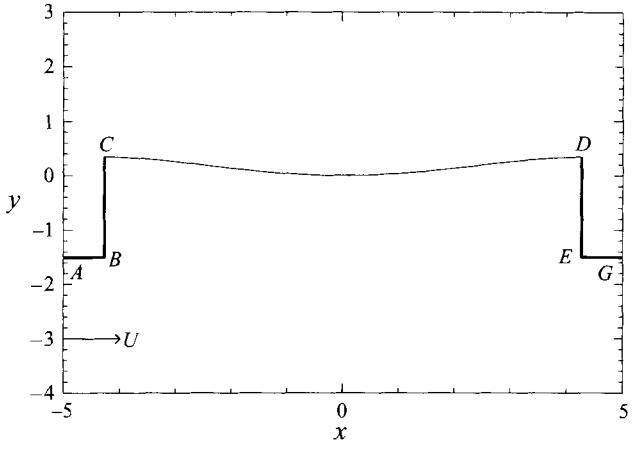

FIGURE 2. Free-surface flow with two stagnation points. This is a computed solution with $P = 2.222$, $\epsilon = 1.147$, $L = 8.696$, $F_l = 0.363$, $H = 0.213$, $C_p = -2.225$.

(B. Molin, personal communication 1996). When the ship is in motion, the fluid motion inside the hole is still poorly understood. In addition to steady motions, two types of sloshing modes have been observed: a piston-like mode in which the whole body of water moves up and down inside the hole, and a standing-wave mode in which there is sloshing inside the hole.

The steady problem is formulated in §2. Two different reformulations based on an integral equation and on a series representation are described in the §§2.1 and 2.2. These reformulations are equivalent but are used in the §§3.1 and 3.2 to derive two different numerical schemes. These numerical approaches are similar to the ones used for example by Vanden-Broeck (1980, 1984), Tuck (1987), Vanden-Broeck & Dias (1992), Dias & Vanden-Broeck (1993) and Moni & King (1995). Solutions are obtained for various values of the parameters and the results are discussed in §§4 and 5. The computations for large distance between the stagnation points reveal an interesting feature of the flow: there is a countably infinite number of solutions and the profiles are wavy.

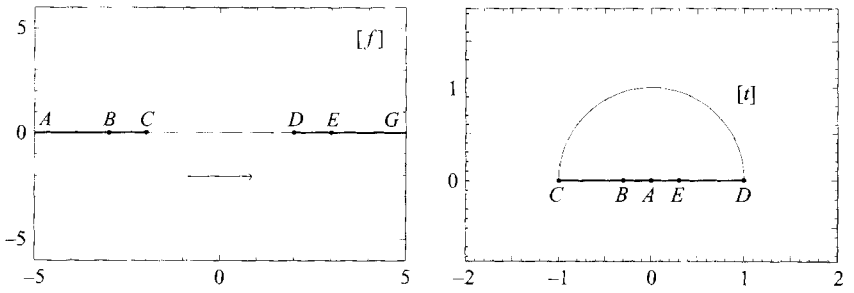

FIGURE 3. The image of the flow of figure 2 in the plane of the complex potential (f-plane) is the lower half-plane. Its image in the t-plane is the upper half-unit disk. The images of the points labelled in figure 2 are shown.

2. Formulation

The flow configuration shown in figure 2 is considered. The flow domain is bounded above by the vertical walls BC and ED and by the horizontal walls AB and EG. The fluid is assumed to be incompressible and inviscid. The flow is assumed to be steady and irrotational. Far downstream the flow is characterized by a uniform stream with a constant velocity U. We choose Cartesian coordinates with the origin on the free surface at an equal distance from the two vertical walls. The flow is assumed to be symmetric with respect to the y-axis. Non-symmetric solutions and solutions where the flow detaches at corner B could be computed as well but are left for future work. We introduce the potential function ϕ and the stream function ψ. Without loss of generality we choose $\psi = 0$ on the free surface and $\phi = 0$ at the origin. The values of the potential function at the points D and E are denoted by ϕ_P and $\phi_P + \phi_K$. It follows from the symmetry of the flow that $\phi = -\phi_P$ and $\phi = -\phi_P - \phi_K$ at the points C and B.

We shall construct solutions for which the points C and D are stagnation points. It can be shown that the free surface is then horizontal at the two points C and D (see Dagan & Tulin 1972).

We define dimensionless variables by taking ϕ_K/U as the unit length and U as the unit velocity. The problem is then characterized by the dimensionless value $P = \phi_P/\phi_K$ of the potential at D and the dimensionless parameters

$$\epsilon = \frac{U^3}{g\phi_K}, \quad L = \frac{Ul}{\phi_K}, \quad F_l = \frac{U}{(gl)^{1/2}}, \quad H = \frac{h}{l}, \quad C_p = \frac{p_{atm} - p_\infty}{\frac{1}{2}\rho U^2}, \tag{2.1}$$

where h denotes the level of the stagnation points above the horizontal walls, l the width between the vertical walls, p_{atm} the pressure along the free surface and p_∞ the pressure at infinity along the horizontal walls.

Next we define the complex velocity $\zeta = u - iv$, where u and v denote the horizontal and vertical components of the velocity. The function ζ is an analytic function of the complex potential f (the flow configuration in the f-plane is shown in figure 3). The free surface is described by $x(\phi)$ and $y(\phi)$. The values of $x(\phi)$ and of $y(\phi)$ can be evaluated in terms of u and v by integrating the identity

$$x_\phi + iy_\phi = \frac{1}{u - iv}. \tag{2.2}$$

On the free surface the pressure is constant. Therefore Bernoulli's equation yields

$$\tfrac{1}{2}\epsilon(u^2+v^2)+y(\phi)=y(P). \tag{2.3}$$

This concludes the formulation of the problem. We seek ζ as an analytic function of f in the lower half-plane $\psi<0$. This function must approach 1 as $\psi\to-\infty$ and satisfy (2.3) on CD and the kinematic conditions

$$u=0 \quad \text{on} \quad BC \quad \text{and} \quad DE \tag{2.4}$$

and

$$v=0 \quad \text{on} \quad AB \quad \text{and} \quad EG. \tag{2.5}$$

Bernoulli's equation yields

$$C_p=1-\frac{2H}{F_l^2}.$$

2.1. *Integral equation reformulation*

In this subsection we reformulate the problem as an integral equation. This is conveniently done by defining the function $\tau-\mathrm{i}\theta$ by

$$\zeta=\mathrm{e}^{\tau-\mathrm{i}\theta}. \tag{2.6}$$

We seek $\tau-\mathrm{i}\theta$ as a function of the complex potential $f=\phi+\mathrm{i}\psi$. This function is also analytic in the lower half-plane $\psi<0$ and vanishes as $\psi\to-\infty$. By using the Cauchy integral formula in the complex potential plane with a contour consisting of the ϕ-axis and a half-circle of arbitrary large radius in the lower half-plane $\psi<0$, we obtain after taking the real part

$$\tau(\phi)=\frac{1}{\pi}\int_{-\infty}^{\infty}\frac{\theta(t)}{t-\phi}\,\mathrm{d}t. \tag{2.7}$$

The integral in (2.7) is a Cauchy principal value.

Using the kinematic conditions (2.4) and (2.5) we have

$$\theta=0 \quad \text{on} \quad AB \quad \text{and} \quad EG, \tag{2.8}$$

$$\theta=\frac{1}{2}\pi \quad \text{on} \quad BC, \tag{2.9}$$

$$\theta=-\frac{1}{2}\pi \quad \text{on} \quad DE. \tag{2.10}$$

Substituting (2.8)–(2.10) into (2.7) we obtain

$$\tau(\phi)=\frac{1}{2}\ln\frac{P^2-\phi^2}{(P+1)^2-\phi^2}+\frac{1}{\pi}\int_{-P}^{P}\frac{\theta(t)}{t-\phi}\,\mathrm{d}t. \tag{2.11}$$

Furthermore the symmetry of the flow implies $\theta(-\phi)=\theta(\phi)$. Thus (2.11) can be rewritten as

$$\tau(\phi)=\frac{1}{2}\ln\frac{P^2-\phi^2}{(P+1)^2-\phi^2}+\frac{1}{\pi}\int_{0}^{P}\theta(t)\left(\frac{1}{t-\phi}+\frac{1}{t+\phi}\right)\mathrm{d}t. \tag{2.12}$$

Substituting (2.6) into (2.3) yields

$$\tfrac{1}{2}\epsilon\,\mathrm{e}^{2\tau}+y(\phi)=y(P). \tag{2.13}$$

This completes the reformulation of the problem. We seek $\tau-\mathrm{i}\theta$ as an analytic function of f in the lower half-plane $\psi<0$, satisfying (2.12) and (2.13).

2.2. *Series expansion reformulation*

In this subsection we present another reformulation using a series representation. The idea is to map the flow domain onto the upper half-unit disk and to expand the complex velocity as a Taylor series inside the unit disk. The image of the free surface is the upper half-unit circle. The image of the solid boundaries is the real diameter.

The mapping of the flow domain from the lower half-plane of the complex potential (f-plane) to the upper half-unit disk (t-plane) is provided by

$$f = \frac{e}{(1-e)^2}\left(t + \frac{1}{t}\right), \tag{2.14}$$

where e denotes the image of the point E in the t-plane (see figure 3). The link between P and e is provided by

$$P = \frac{2e}{(1-e)^2}. \tag{2.15}$$

Next the complex velocity ζ is expanded as

$$\zeta = (1-t^2)(e^2-t^2)^{-1/2}\sum_{n=0}^{+\infty} a_n t^{2n}. \tag{2.16}$$

This expansion factors out the singular behaviour of the velocity at the corners E and B ($t = \pm e$) and the singular behaviour of the velocity at the stagnation points D and C ($t = \pm 1$). Moreover, the expansion takes advantage of the symmetry of the problem. At $t = 0$, the velocity approaches unity. Therefore

$$a_0 = e. \tag{2.17}$$

Bernoulli's equation (2.3) is rewritten as

$$\epsilon|\zeta|^2 + 2y = 2y|_{t=\pm 1}. \tag{2.18}$$

Parameterizing the free surface by

$$t = \mathrm{e}^{\mathrm{i}\sigma}, \quad 0 \leqslant \sigma \leqslant \pi,$$

and differentiating (2.18) with respect to σ leads to

$$\epsilon[u(\sigma)u_\sigma(\sigma) + v(\sigma)v_\sigma(\sigma)] - P\sin\sigma\frac{v(\sigma)}{u^2(\sigma)+v^2(\sigma)} = 0. \tag{2.19}$$

We note the identity

$$\frac{P^2-f^2}{(P+1)^2-f^2} = \frac{e(1-t^2)^2}{(e^2-t^2)(1-e^2t^2)}. \tag{2.20}$$

This completes the reformulation of the problem. The coefficients a_n in (2.16) are sought such that (2.19) is satisfied.

3. Numerical results

We now describe two different numerical schemes based on the integral equation reformulation and the series expansion reformulation of §2. Preliminary calculations based on these schemes have shown that the two parameters ϵ and P cannot be specified independently. Here we present the final version of the schemes in which P is given and ϵ is found as part of the solution.

3.1. *Integral equation reformulation*

In this section, we solve the system (2.12), (2.13) numerically.

First we introduce the mesh points

$$\phi_I = \frac{P(I-1)}{N-1}, \quad I = 1,\ldots,N \tag{3.1}$$

and the midpoints

$$\phi_{I-1/2} = \tfrac{1}{2}(\phi_{I+1} + \phi_I), \quad I = 1,\ldots,N-1. \tag{3.2}$$

$(N+1)$ unknowns are introduced: ϵ and

$$\theta_I = \theta(\phi_I), \quad I = 1,\ldots,N. \tag{3.3}$$

Equation (2.12) is evaluated at the midpoints $\phi_{I-1/2}, I = 1,\ldots,N-1$. The Cauchy principal value is evaluated by the trapezoidal rule with a summation over the mesh points $\phi_J, J = 1,\ldots,N$. The symmetry of the quadrature and of the discretization enables us to evaluate the Cauchy principal value as if it were an ordinary integral. This gives the values of τ at the midpoints.

Next we evaluate the values of $y(\phi)$ and $x(\phi)$ at the midpoints by integrating numerically (2.2).

We obtain $(N-2)$ algebraic equations by satisfying (2.13) at the midpoints (3.2), except at $\phi_{1/2}$. Two more equations are obtained by imposing the conditions

$$\theta_1 = \theta_N = 0. \tag{3.4}$$

The last equation expresses the value of θ_1 in terms of $\theta_2, \theta_3, \theta_4$ by a three-point extrapolation formula.

For a given value of P, this leads to a system of $(N+1)$ nonlinear algebraic equations for the $(N+1)$ unknowns. This system is solved numerically by Newton's method.

3.2. *Series expansion reformulation*

The problem is solved numerically by truncating the infinite series in (2.16) after $(N-1)$ terms. Next we introduce the $(N-1)$ mesh points on the free surface

$$\sigma_I = \frac{(I-\frac{1}{2})\,\pi}{N-1\ 2}, \quad I = 1,\ldots,N-1. \tag{3.5}$$

We satisfy the equation (2.19) at the mesh points (3.5). This yields $(N-1)$ equations for the following N unknowns: ϵ and $a_n, n = 0,\ldots,N-2$. The last equation simply is (2.17). For a given value of P (or e equivalently), this system of N nonlinear equations with N unknowns is solved by Newton's method.

4. Discussion of the results

The schemes described in the previous section were used to compute solutions for various values of ϵ and P. The numerical results obtained by the integral equation scheme were found to be in good agreement with those obtained by the series expansion scheme. This constitutes a check on both schemes. The integral equation scheme is more general and worked for all the solutions described in this Section. The series expansion scheme is more efficient (i.e. accurate solutions can be computed with N relatively small), but it is not well suited to solutions with a large number of waves.

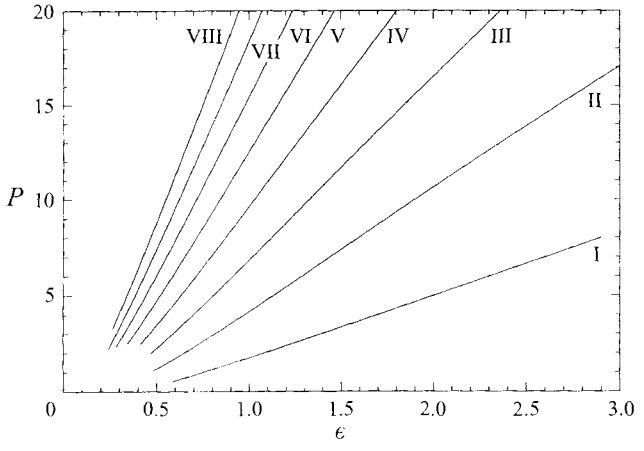

FIGURE 4. Free-surface flows with two stagnation points. Computed solutions in the (P, ϵ)-plane. The branches are labelled I, II, etc., counterclockwise. The label is the number of waves present on the free surface for large values of P.

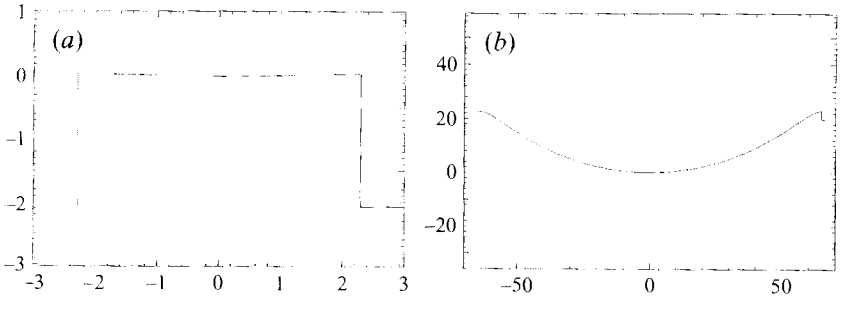

FIGURE 5. Free-surface flows with two stagnation points. Computed solutions on branch I with $P = 0.5354$, $\epsilon = 0.588$, $L = 4.67$, $F_l = 0.355$, $H = 0.452$, $C_p = -6.19$ (a) and $P = 75.56$, $\epsilon = 22.14$, $L = 131.4$, $F_l = 0.41$, $H = 0.025$, $C_p = 0.70$ (b).

Values of P versus ϵ are presented in figure 4. These results show that for each value of ϵ, there is a solution for only a discrete set of values of P. Each curve in figure 4 defines a branch of solutions. It is convenient to label these branches I, II, etc., counterclockwise. Although we have only computed eight branches of solutions, we expect that there is a countably infinite number of them.

Free-surface profiles corresponding to branches I–VIII are presented in figures 5–9. The profile shown in figure 2 belongs to branch I. Figures 5–9 show that there is a train of waves on the free surface and that the label of a family is equal to the number of waves between the two vertical walls. For solutions with small-amplitude waves, it was checked that the wavelength is approximately equal to the wavelength $2\pi\epsilon$ of small-amplitude waves in deep water with phase velocity U.

Several quantities of interest are found as part of the solution: they are the dimensionless width L between the vertical walls, the Froude number F_l based on l, the pressure coefficient C_p, and the ratio h/l (see (2.1)).

Since the change of width for a given P was found to be small as one moves from one branch to the other, it is clearer to present the graph of $L_0 - L$ versus P for the different branches, where L_0 denotes the length corresponding to $\epsilon = 0$ for the

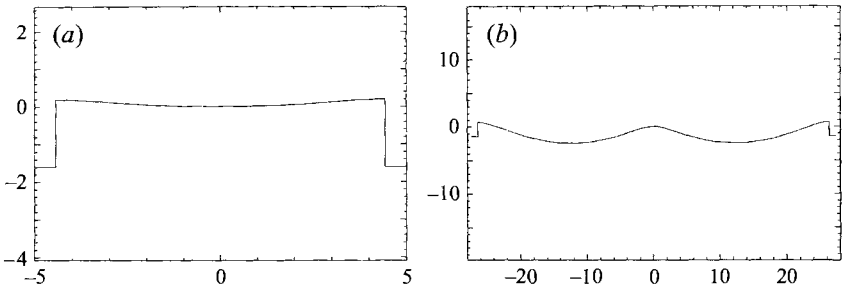

FIGURE 6. Free-surface flows with two stagnation points. Computed solutions on branch II with $P = 2.35$, $\epsilon = 0.704$, $L = 9.02$, $F_l = 0.280$, $H = 0.199$, $C_p = -4.09$ (a) and $P = 25$, $\epsilon = 4.29$, $L = 53.37$, $F_l = 0.283$, $H = 0.041$, $C_p = -0.019$ (b).

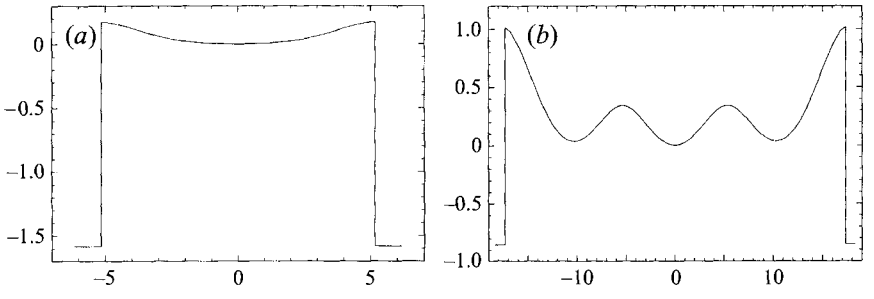

FIGURE 7. Free-surface flows with two stagnation points. Computed solutions on branch III with $P = 3$, $\epsilon = 0.586$, $L = 10.49$, $F_l = 0.236$, $H = 0.168$, $C_p = -5.00$ (a) and $P = 15$, $\epsilon = 1.84$, $L = 35.08$, $F_l = 0.229$, $H = 0.054$, $C_p = -1.04$ (b). The vertical scale is exaggerated.

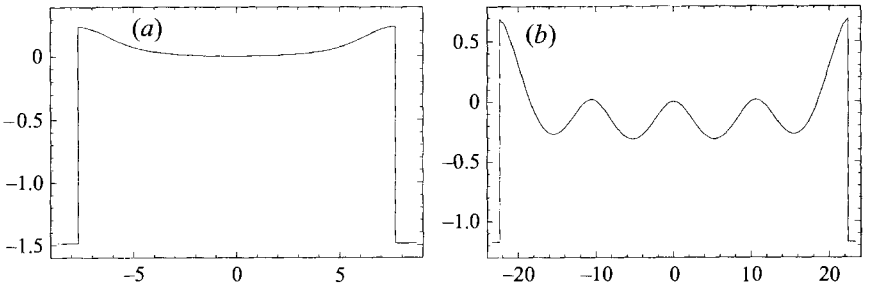

FIGURE 8. Free-surface flows with two stagnation points. Computed solutions on branch IV with $P = 5.35$, $\epsilon = 0.66$, $L = 15.57$, $F_l = 0.206$, $H = 0.111$, $C_p = -4.25$ (a) and $P = 20$, $\epsilon = 1.80$, $L = 45.25$, $F_l = 0.20$, $H = 0.041$, $C_p = -1.08$ (b). The vertical scale is exaggerated.

same value of P. When $\epsilon = 0$, the free surface is flat (see (2.13)) and $\theta(\phi) = 0$ for $-P < \phi < P$. Therefore (2.12) gives

$$\tau_0(\phi) = \frac{1}{2} \ln \frac{P^2 - \phi^2}{(P+1)^2 - \phi^2}.$$

It is easy to integrate (2.2) to obtain

$$L_0 = 2 \int_0^P \left[\frac{(P+1)^2 - \phi^2}{P^2 - \phi^2} \right]^{1/2} \mathrm{d}\phi.$$

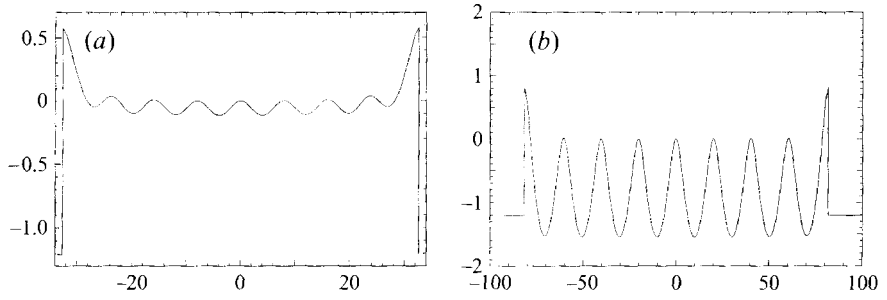

FIGURE 9. Free-surface flows with two stagnation points. Computed solutions on branch VIII with $P = 30$, $\epsilon = 1.34$, $L = 65.8$, $F_l = 0.143$, $H = 0.027$, $C_p = -1.69$ (*a*) and $P = 80$, $\epsilon = 3.405$ (*b*). The vertical scale is exaggerated.

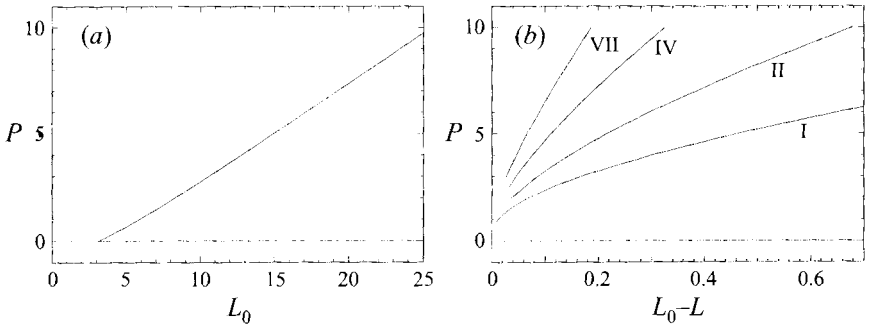

FIGURE 10. Distance between vertical walls as a function of P: (*a*) L_0 corresponding to $\epsilon = 0$, (*b*) $L_0 - L$ along the branches I, II, IV, VII (counterclockwise).

L_0 is plotted in figure 10(*a*) while $L_0 - L$ is plotted in figure 10(*b*).

Figure 11 shows a plot of F_l versus h/l. Along each branch of solution, the Froude number is almost constant. This result is similar to the result for periodic gravity waves. For such waves, the Froude number based on the wavelength $l = 2\pi/k$,

$$F_l = U\left(\frac{k}{2\pi g}\right)^{1/2},$$

is equal to 0.3989 for infinitesimal waves and to 0.4358 for the highest waves. If there are n waves confined in the distance l, F_l must be divided by $n^{1/2}$. Figure 12 shows a plot of C_p versus h/l. It is interesting to note that blowing-type solutions with $C_p > 0$ are possible only along branch I. All other solutions are suction-type solutions with $C_p < 0$. All branches except branch I end close to $C_p = 0$, which corresponds to $F_l^2 = 2H$. The curve $C_p = 0$ has been added in figure 11.

As P increases along a branch, the waves on the free surface increase in amplitude. The behaviour of the solutions for P large is described in detail in the next Section.

As P decreases along a branch, the waves ultimately become of extremely small amplitude and can no longer be seen on the profiles (see part (*a*) in figures 5–9). For each branch shown in figure 4, we had to stop our calculations at some value of P because our scheme became sensitive for smaller values of P. What happens for smaller values of P still is an open problem: in order to study precisely what happens an analytical approach or perhaps a code with exponential accuracy should be used.

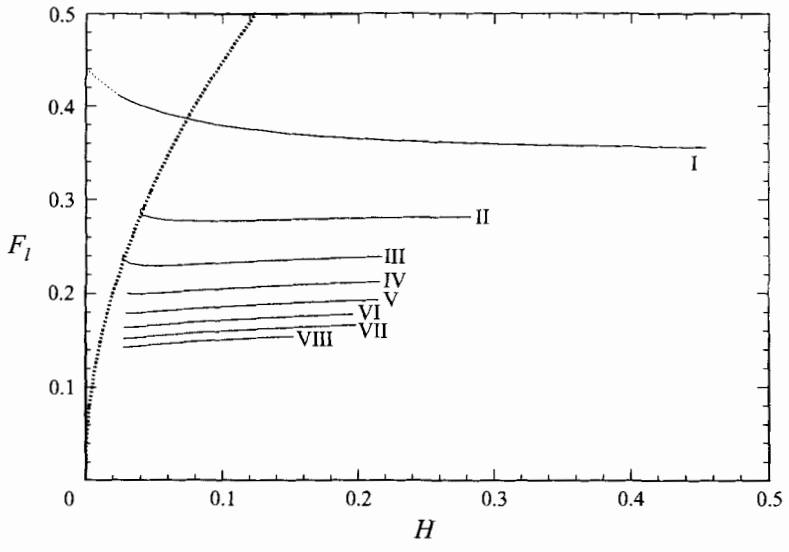

FIGURE 11. Froude number F_l based on the width l between the vertical walls as a function of H. The dotted line along branch I represents an extrapolation between the last computed point and the infinite-P limit. The thick dotted line is the curve $C_p = 0$. The labelling of the curves is the same as in figure 4.

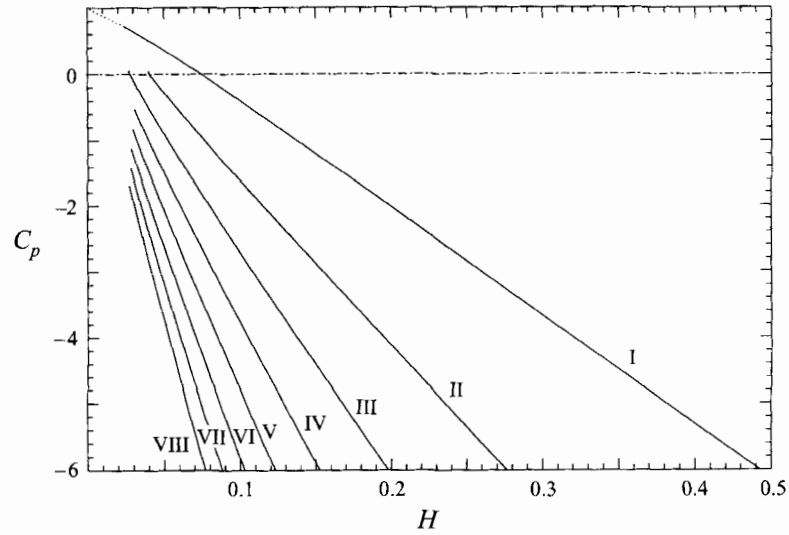

FIGURE 12. Pressure coefficient C_p versus H. The labelling of the curves is the same as in figure 4.

Our solutions are expected to approach asymptotically the stern flows of Vanden-Broeck & Tuck (1977) and Vanden-Broeck, Schwartz & Tuck (1978) as the label of the families tends to infinity. To check this, we consider branch VIII. Figure 9 shows two computed solutions with $P = 30$ and $P = 80$. The profile with $P = 80$ for x negative is similar to the stern flow shown in figure 1 of Vanden-Broeck (1980). In figure 2 of his paper, Vanden-Broeck (1980) gives the value of the steepness of waves versus the draught-based Froude number (the draught is defined as the distance between the horizontal wall and the level of the free surface at which the velocity is

Branch	P	a_1	a_{10}	a_{20}	a_{30}
I	0.5354	-1.6×10^{-3}	0	0	0
I	40	-0.11	-1.6×10^{-4}	-7.2×10^{-7}	-4.7×10^{-9}
VIII	8	0.10	-4.3×10^{-5}	5.9×10^{-9}	-2.5×10^{-11}
VIII	20	0.17	-4.1×10^{-3}	2.7×10^{-5}	8.0×10^{-7}

TABLE 1. Decay of coefficients of the series (2.16). Zero coefficients are coefficients with an absolute value smaller than the machine accuracy.

equal to U). We computed the draught-based Froude number and the steepness of the waves for the solutions of branch VIII and found that these values agree with the broken curve of figure 2 in Vanden-Broeck (1980) for P sufficiently large. The draught-based Froude number corresponding to $P = 80$ is equal to 3.22.

Regarding accuracy, we have checked that increasing the number of points (200, 400, 600) does not change the results for the integral formulation, except near the critical region (i.e. for P small). For P large on branches with a high label, a large number of points is required. In the series truncation method, it was found that the coefficients in the series decrease quite rapidly (see table 1).

5. Solutions for large values of P

5.1. *Branch I*

As P increases, the height of the wall becomes small with respect to the amplitude of the wave (see figure 5*b*). The parameters used so far are not appropriate to deal with large values of P. Better parameters are

$$\varepsilon = \frac{\epsilon}{P}, \quad \mathscr{L} = \frac{L}{P}. \tag{5.1}$$

These new parameters essentially arise by taking ϕ_P as unit potential rather than ϕ_K. Figure 13 shows the variation of $\mathscr{L}$ as a function of ε along the upper part of branch I. The results for large P along branch I seem to indicate that flows still with two stagnation points but without corners can be computed. It is the subject of this subsection to compute such limiting configurations. We shall construct a solution for which the points C and D still are stagnation points but the angle between the free surface and the wall now is $2\pi/3$. We use a scheme based on a series expansion. The mapping of the flow domain from the lower half-plane of the complex potential (f-plane) to the upper half-unit disk (t-plane) is provided by

$$f = \frac{1}{2}\left(t + \frac{1}{t}\right). \tag{5.2}$$

Next we expand the complex velocity ζ as

$$\zeta = (1 - t^2)^{2/3} \sum_{n=0}^{+\infty} a_n t^{2n}. \tag{5.3}$$

This expansion factors out the leading singular behaviour of the velocity at the stagnation points D and C ($t = \pm 1$). There are lower-order singularities at $t = \pm 1$

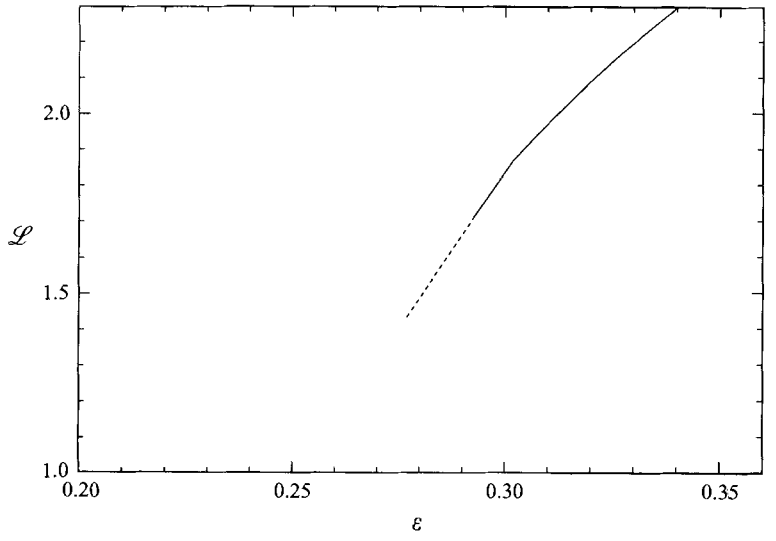

FIGURE 13. Plot of $\mathscr{L}$ versus ε along the upper part of branch I. The dotted line represents an extrapolation between the last computed point ($P = 75.56$) and the infinite-P limit.

(see Grant 1973). However in spite of these singularities, the function

$$\frac{\zeta}{(1-t^2)^{2/3}}$$

is analytic in $|t| < 1$ and continuous in $|t| \leqslant 1$ and can be expanded in powers of t (see Vanden-Broeck & Tuck 1994). Moreover, the expansion takes advantage of the symmetry of the problem. At $t = 0$, the velocity approaches unity. Therefore $a_0 = 1$. The problem was solved numerically by truncating the series in (5.3) after a finite number of terms as in §3.2. A unique solution was found. The corresponding values of the parameters are $\varepsilon = 0.277$ and $\mathscr{L} = 1.432$. These values have been added to figures 11, 12 and 13. The corresponding profile is shown in figure 14.

5.2. *Branch II*

Using the expansion (5.3), we tried to compute solutions with two waves but were not successful. What happens is that the two-wave profiles (i.e. the solutions along branch II) develop a stagnation point in the middle as P increases. This limiting profile is reached before P reaches infinity. Indeed, the programs (both integral and series) failed to converge for values of P above $P = 26$ along branch II. The complex velocity ζ is then expanded as

$$\zeta = (1-t^2)(e^2-t^2)^{-1/2}(1+t^2)^{1/3}\sum_{n=0}^{+\infty} a_n t^{2n}. \tag{5.4}$$

This expansion factors out the leading singular behaviour of the velocity at the stagnation points D, C ($t = \pm 1$) and in the middle of the free surface ($t = i$). Moreover, the expansion takes advantage of the symmetry of the problem. At $t = 0$, the velocity approaches unity. Therefore $a_0 = e$. A unique solution was found. The corresponding values of the parameters are $e = 0.762$, $P = 26.8$, $\varepsilon = 0.176$ and $\mathscr{L} = 2.09$. The corresponding profile is shown in figure 15.

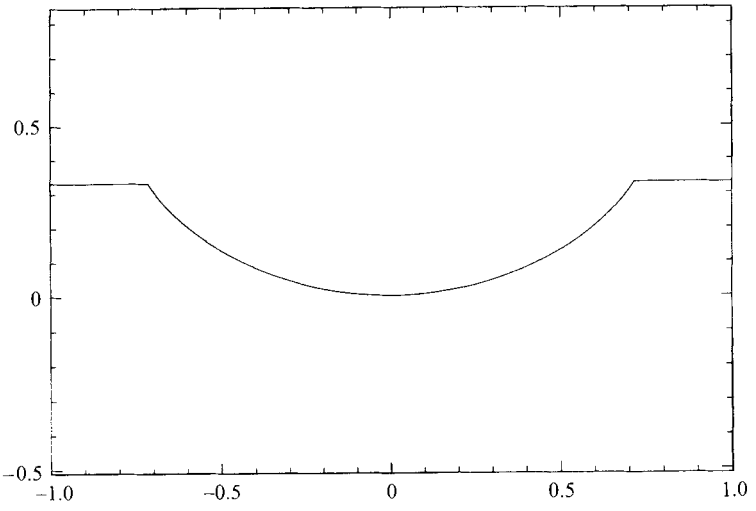

FIGURE 14. Free-surface flow corresponding to the limit on branch I as P goes to infinity. The Froude number F_l is equal to 0.44.

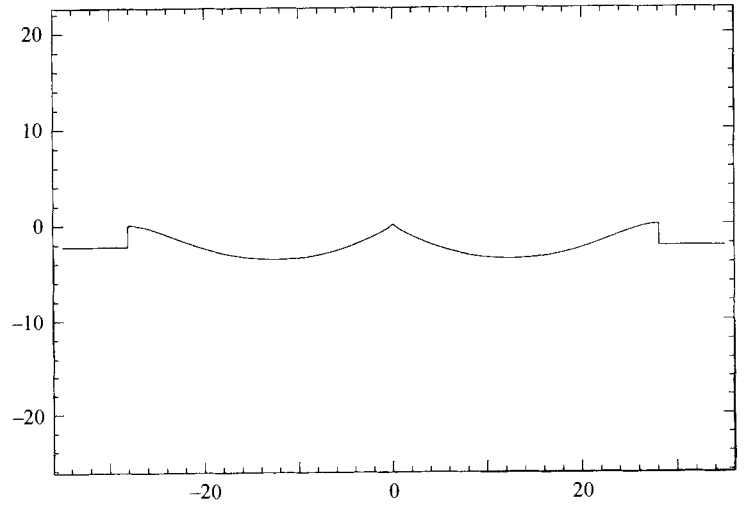

FIGURE 15. Limiting solution along branch II. The corresponding values for P and F_l are 26.8 and 0.290.

5.3. *Branch III*

For branch III, we assumed the limiting configuration to be one with four stagnation points, two on the walls and two symmetric ones along the free surface. The complex velocity ζ is expanded as

$$\zeta = (1-t^2)(e^2-t^2)^{-1/2}[(1+t^2)^2 - 4t^2\cos^2\gamma]^{1/3}\sum_{n=0}^{+\infty} a_n t^{2n}, \tag{5.5}$$

where γ and $\pi-\gamma$ are the angles in the t-plane of the unknown stagnation points. This expansion factors out the leading singular behaviour of the velocity at the stagnation points D, C ($t = \pm 1$) and at the two symmetric points along the free surface whose

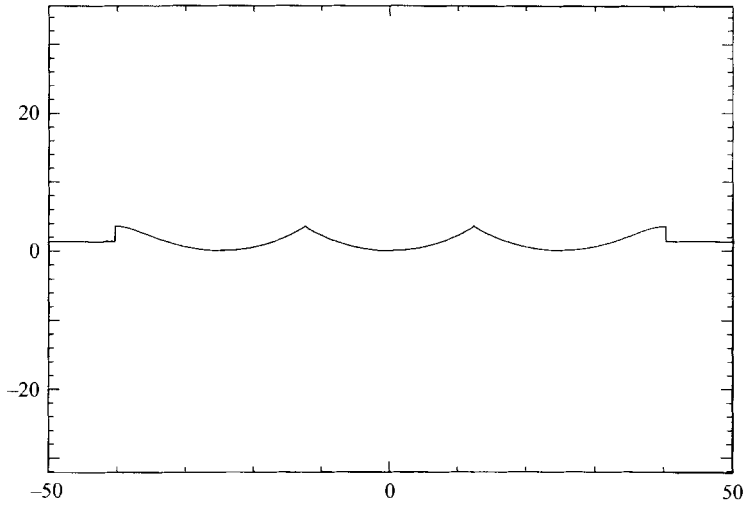

FIGURE 16. Limiting solution along branch III. The corresponding values for P and F_l are 39.0 and 0.241.

location is unknown. Moreover, the expansion takes advantage of the symmetry of the problem. At $t = 0$, the velocity approaches unity. Therefore $a_0 = e$. A unique solution was found. The corresponding values of the parameters are $e = 0.8$, $\gamma = 1.24$, $P = 39$, $\varepsilon = 0.12$ and $\mathscr{L} = 2.1$. The corresponding profile is shown in figure 16.

The work of the first author was supported in part by the National Science Foundation, as well as the Lady Davis Foundation. He gratefully acknowledges the hospitality of the Hebrew University of Jerusalem, Tel Aviv University and the Technion. The computations presented in this work were performed on the CRAY YMP-2E vector supercomputer located at IMT (Institut Méditerranéen de Technologie - Marseille - France), and were funded by Conseil Régional Provence-Alpes-Côte d'Azur.

REFERENCES

DAGAN, G. & TULIN, M. P. 1972 Two-dimensional free-surface gravity flow past blunt bodies. *J. Fluid Mech.* **51**, 529–543.

DIAS, F. & VANDEN-BROECK, J.-M. 1993 Nonlinear bow flows with spray. *J. Fluid Mech.* **255**, 91–102.

GRANT, M. A. 1973 The singularity at the crest of a finite amplitude progressive Stokes wave. *J. Fluid Mech.* **59**, 257–262.

MONI, J. N. & KING, A. C. 1995 Interfacial solitary waves. *Q. J. Mech. Appl. Maths* **48**, 21–38.

TUCK, E. O. 1987 Efflux from a slit in a vertical wall. *J. Fluid Mech.* **176**, 253–264.

VANDEN-BROECK, J.-M. 1980 Nonlinear stern waves. *J. Fluid Mech.* **96**, 603–611.

VANDEN-BROECK, J.-M. 1984 Rising bubbles in a two-dimensional tube with surface tension. *Phys. Fluids* **27**, 2604–2607.

VANDEN-BROECK, J.-M. & DIAS, F. 1992 Solitary waves in water of infinite depth and related free surface flows. *J. Fluid Mech.* **240**, 549–557.

VANDEN-BROECK, J.-M., SCHWARTZ, L. W. & TUCK, E. O. 1978 Divergent low-Froude-number series expansion in nonlinear free-surface flow problems. *Proc. R. Soc. Lond.* A **361**, 207–224.

VANDEN-BROECK, J.-M. & TUCK, E. O. 1977 Computation of near-bow or stern flows, using series expansion in the Froude number. In *Proc. 2nd Intl Conf. on Numerical Ship Hydrodynamics, Berkeley, CA*, pp. 371–381. University Extension Publications.

VANDEN-BROECK, J.-M. & TUCK, E. O. 1994 Flow near the intersection of a free surface with a vertical wall. *SIAM J. Appl. Maths* **54**, 1–13.